Mitigating the effects of choroidal hyper- and hypo-transmission defects on choroidal vascularity index assessments using optical coherence tomography

Hao Zhou[1]^, Jie Lu[1], Kelly Chen[1], Yingying Shi[2], Giovanni Gregori[2], Philip J. Rosenfeld[2], Ruikang K. Wang[1,3]

[1]Department of Bioengineering, University of Washington, Seattle, WA, USA; [2]Department of Ophthalmology, Bascom Palmer Eye Institute, University of Miami Miller School of Medicine, Miami, FL, USA; [3]Department of Ophthalmology, University of Washington, Seattle, WA, USA

Contributions: (I) Conception and design: H Zhou, RK Wang; (II) Administrative support: H Zhou, Y Shi, G Gregori, PJ Rosenfeld, RK Wang; (III) Provision of study materials or patients: Y Shi, G Gregori, PJ Rosenfeld; (IV) Collection and assembly of data: Y Shi, G Gregori; (V) Data analysis and interpretation: H Zhou, J Lu, K Chen, Y Shi, PJ Rosenfeld, RK Wang; (VI) Manuscript writing: All authors; (VII) Final approval of manuscript: All authors.

Correspondence to: Prof. Ruikang K. Wang, PhD. Bioengineering & Ophthalmology, University of Washington, Box 355061, 3720 15th Ave NE, Seattle, WA 98195-5061, USA. Email: wangrk@uw.edu.

Background: Changes in choroidal vascularity index (CVI) are associated with multiple choroid-related ocular diseases. CVI is calculated as the area/volume ratio of vessels in the choroid, which could be affected by alterations in regional signal intensities due to hypo-transmission defects (hypoTDs) caused by drusen and retinal pigment epithelium (RPE) detachments, and hyper-transmission defects (hyperTDs) caused by the absence of RPE. To develop a simulation model to verify the CVI assessments in eyes with hyper/hypoTDs and demonstrate that accurate CVIs can be achieved after attenuation correction on swept-source optical coherence tomography (SS-OCT).

Methods: A simulation model was developed on 6×6 mm macular scans from normal subjects. Signal intensity in a cylindrical region below RPE was altered to mimic hyper/hypoTDs. CVIs were compared inside and outside the simulated regions before and after attenuation correction. CVI assessments of OCT scans from patients with hyperTDs due to geographic atrophy (GA) and from patients with hypoTDs due to drusen that subsequently resolved with the disappearance of the hypoTDs were compared with and without attenuation correction.

Results: Ten normal eyes were recruited to generate the hyper/hypoTD simulation model. In eyes with hypoTDs, CVIs were overestimated, and in eyes with hyperTDs, the CVIs were underestimated (P<0.001). After attenuation correction, the uneven distribution of signal intensity was eliminated and the resulting CVI showed no significant difference compared with the 'ground truth', which is measured from the original scans. Attenuation correction successfully eliminated the influence of hyperTDs caused by GA on CVI measurements (n=38). Quantitatively, no significant difference was found in the CVIs of eyes before and after drusen collapse with attenuation correction (n=8).

Conclusions: The simulation model could reveal the impact of hypo/hyperTDs on CVI quantification in eyes with choroid-involved ocular diseases. The importance of attenuation correction to ensure accuracy in choroidal vessel segmentation was demonstrated by analyzing eyes with GA or drusen.

Keywords: Choroidal vessel quantification; choroidal vascularity index (CVI); choroidal hyper/hypo-transmission defect; geographic atrophy (GA); drusen

---

^ ORCID: 0000-0003-0068-5102.

Introduction

The choroid is a layer comprised of dense blood vessels located between the retina and sclera, and is mainly responsible for delivering nutrients and supporting the metabolic exchange between the circulation and the retinal pigment epithelium (RPE) and photoreceptors (1-3). Alterations in choroidal thickness and choroidal blood vessels may play key roles in the development of chorioretinal diseases (4-7). Recent developments of optical coherence tomography (OCT) have enabled the imaging of choroid (5,8). Measurements of the choroidal vasculature relative to the surrounding stroma is now known as the choroidal vascularity index (CVI), which is defined as the area/volume ratio of vessel lumen to the entire choroid (9,10). An increased CVI has been associated with central serous chorioretinopathy (CSCR) and Vogt-Koyanagi-Harada (VKH), while a reduced ratio has been associated with age-related macular degeneration (AMD), polypoidal choroidal vasculopathy (PCV), diabetes mellitus, retinitis pigmentosa and inflammatory conditions (11-18).

Choroidal vessel segmentation has been explored with various local or global thresholding methods, however, it is hindered by the lack of a "ground truth". An accurate CVI measurement requires the appropriate segmentation of choroidal vessels, which typically appear as hyporeflective lumens in the choroidal slab of clinical OCT images (19). Manual segmentation of the dark lumen in the choroidal slab has been used, but only relatively large vessels in a very limited number of OCT B-scans have been labeled routinely due to the poor contrast of the images and the need for labor-intensive annotation of the images (20). A bias in the subjective grading across observers were also reported on choroidal images with high and low contrast (21). Automatic segmentation of the choroidal images is necessary to perform such time-/labor-consuming work, especially when working with the entire 3D OCT dataset consisting of subfoveal B-scans (22). However, when a previous study compared the CVI measurements from two commonly adopted binarization algorithms on 100 normal eyes, poor agreement was found between the two methods (23). The study failed to identify which of the methods gave the most accurate CVI or was better at identifying choroidal

vessels. When it comes to the choroid in eyes with pathologies such as GA and drusen, it becomes even more challenging to evaluate the true change of CVI, given the potential bias caused by the method itself and additional biases introduced by overlying pathologies in the retina and along the RPE.

Among the factors that may potentially influence the accuracy of CVI measurements, regional alterations in signal intensities are probably the most important since all the current vessel segmentation methods are based on signal intensity thresholding (9,24). Choroidal hyper- and hypo-transmissions defects (hyper/hypo-TDs) occur when there are abnormalities or damage to the RPE/Bruch's membrane (BM) complex (25). HypoTDs arise when the choroidal OCT signal is diminished under regions with overlying features that attenuate the OCT signal such as pigmentary hyper-reflective material, blood, or an elevation of the RPE known as a retinal pigment epithelial detachment (PED). Compared with the surrounding tissue, the choroidal regions that underlie structures causing signal attenuation appear as areas with choroidal hypo-transmission (*Figure 1A*). On the other hand, the choroid under regions where RPE layer is disrupted or absent would present a higher OCT signal relative to the surrounding tissue, such choroidal hyper-transmission is a typical signs of geographic atrophy (GA) or tears of the RPE (*Figure 1B*). Since the dark lumens in the choroid are segmented through thresholding methods, the altered signal strength will influence the intensity distribution of signals, leading to inaccurate CVIs values.

It has long been clear that hyper/hypoTDs associated with features such as drusen, PEDs, pigment aggregations, and GA could affect the quantification of choriocapillaris flow deficits because of their effect on the OCT angiographic signals (26), and researchers have typically either excluded regions with hyper/hypoTDs or applied compensation methods before image binarization (26,27). However, there has been no reports on how these hyper/hypoTDs affect the identification of choroidal vessels. Although hyper/hypoTDs can always be excluded when measuring CVI, this is an unsatisfactory approach, as it ignores possible focal or regional differences in the choroidal vasculature within the areas of the hyper/hypoTDs that are associated with certain
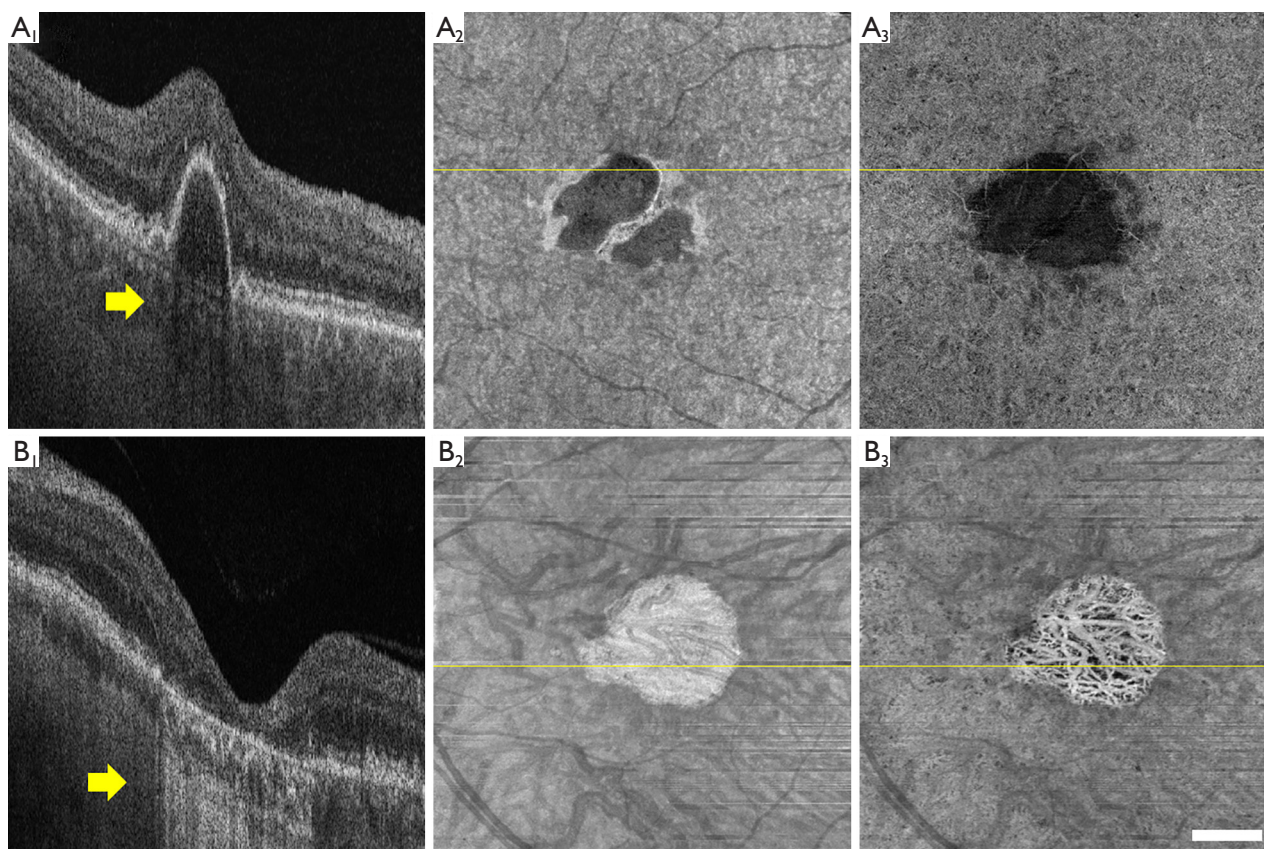
Figure 1 The choroidal hyper/hypoTD. Examples of (A) an eye with drusenoid PED showing choroidal hypo-transmission (arrow) and (B) an eye with GA showing choroidal hyper-transmission (arrow) on B-scans; (A1,B1) location indicated by yellow lines), enface OCT images (A2,B2) and enface OCTA images (A3,B3) of a sub-RPE slab extending from 40 to 150 µm beneath BM respectively. Scale bar: 1 mm. HypoTD, hypo-transmission defect; PED, pigment epithelium detachment; GA, geographic atrophy; OCT, optical coherence tomography; OCTA, optical coherence tomography angiography; RPE, retinal pigment epithelium; BM, Bruch's membrane.

diseases. The question arises as to whether these hyper/hypoTDs can be compensated when measuring the CVI and whether a standard approach can be developed when using different algorithms to measure the CVI in eyes with hyper/hypoTDs.

We previously developed a method to automatically quantify the choroid using the entire swept-source optical coherence tomography (SS-OCT) 3D dataset after attenuation correction (28). We also studied normal eyes over a wide range of ages and identified the normal 95% confidence range of CVI for assessing the 3D choroidal vasculature (10). Attenuation correction can increase the inter-layer contrast leading to more accurate segmentation of the choroid and choroidal vessels, and can eliminate the intra-layer differences, reducing the shadowing effects from large retinal vessels (29). In this study, we designed

a simulation model of choroidal hyper/hypoTDs when using SS-OCT scans from normal eyes to demonstrate how hyper/hypoTDs might affect CVI quantification. The CVI measurements from the original scans of normal eyes served as the "ground truth" when we investigated whether the attenuation correction method adequately compensated for our simulated hyper/hypoTDs regions. We also evaluated the CVI measurements from eyes with GA and drusen with and without attenuation correction. We present the following article in accordance with the MDAR checklist (available at https://qims.amegroups.com/article/view/10.21037/qims-21-1093/rc).

Methods

The study was conducted in accordance with the

Declaration of Helsinki (as revised in 2013). The study was approved by the Institutional Review Board (IRB) of Medical Sciences Subcommittee at the University of Miami, Miller School of Medicine and written informed consent was taken from all individual participants.

Imaging acquisition

One 6×6 mm macular scan of each enrolled eye was obtained using a SS-OCT instrument (PLEX Elite 9000; Carl Zeiss Meditec, Inc., Dublin, California, USA) with a scanning rate of 100,000 A-scans per second and a swept source laser with a central wavelength of 1,050 nm. Scans with a signal strength less than 7 or with motion artifacts were excluded. Each 6×6 mm scan consisted of 500 B-scans, repeated twice at each B-scan location, and each B-scan consisted of 500 A-scans.

CVI measurement

CVI was measured as the ratio of choroidal vessels volume to choroidal volume in the entire choroidal slab using a previously reported automated method (10,28). The choroidal slab extended from BM to the envelope of the outer boundary of choroidal vessels. These layers were automatically segmented using a validated lab-built software (28) and manually corrected through user-guided software when necessary (30). Choroidal vessels were binarized using the Otsu's method from each B-scan using a validated lab-built software (28,31). The method of attenuation correction has also been reported previously and was applied to study the effect of attenuation correction on CVI measurement (28). The same segmentation for choroidal slabs was used when comparing CVI measurement before and after attenuation correction.

Hyper/hypoTD simulation model

In order to demonstrate the impact of hyper/hypoTD on CVI measurement, we simulated the effect of hyper/hypoTDs on scans of normal eyes and used the CVI calculated from the original scan as the 'ground truth'. Normal subjects were recruited and SS-OCT scan of one eye from each subject was entered in the study.

To generate the hyper/hypoTD simulation model, each SS-OCT scan was flattened at the BM boundary and the signal intensity in a cylindrical region below BM was altered using a hyper/hypo-transmission ratio (hyper/hypoTR) to

mimic hyper/hypoTDs.

$$I'_{(x,y)<r,Z>Z_{BM}} = I_{0(x,y)<r,Z>Z_{BM}} \times hyper/hypoTR \quad [1]$$

where I_0 is the original intensity of the pixel in linear display, r is the radius of the circle centered at fovea, (x, y) < r represent all the pixels inside the circle, Z is the depth location of a pixel and ZBM is the depth location of BM on each A-scan. Hyper/hypoTR assumed values between 0.7 and 1.3 while the diameter of the lesion at fovea was set to vary between 300 and 2,700 μm (*Figure 2*). When the hyper/hypoTR was larger than 1, it simulated the choroidal hyper-transmission, otherwise it simulates the choroidal hypo-transmission.

The alterations in the A-scan signal at the choroid cause an imbalance in the total energy of the A-scans in the 3D image. To compensate for this issue, the OCT signals in a 50 pixel (100 μm-thick) slab above BM which approximately corresponds to the RPE/BM complex was adjusted to ensure a consistent total signal intensity in each A-scan. We used

$$I'_{(x,y)<r,Z_{BM-50}<Z<Z_{BM}}$$
$$= I_{0(x,y)<r,Z_{BM-50}<Z<Z_{BM}} \times \frac{\sum I_{0(x,y)<r,Z>Z_{BM-50}} - \sum I'_{(x,y)<r,Z<Z_{BM}}}{\sum I_{0(x,y)<r,Z_{BM-50}<Z<Z_{BM}}} \quad [2]$$

where (x,y) < r, $Z_{BM-50} < Z < Z_{BM}$ represents the pixels inside a 50-pixel slab above the cylindrical region. Background noise level was determined using the intensities of pixels in the vitreous. In pixels where the adjusted signal intensity fell below background noises the signal was given a random value consistent with the noise level. In pixels where the adjusted signal intensity rose above saturation level the signal was set to the highest value (which is 255 in 0–255 greyscale display).

Signal distributions in the choroidal slab inside and outside the simulated hyper/hypoTD regions were compared. CVI *en face* maps were generated by calculating the ratio of the numbers of pixels in vessel lumen and pixels in the choroidal slab in each A-scan. CVI was measured inside and outside the hyper/hypoTD regions, on both normal scans and simulated scans, with and without attenuation correction. CVIs calculated from the original normal scans were used as the 'ground truth' and correlations between severity of hyper/hypoTR and CVI were studied.

CVI measurements in clinical cases with hyper/hypoTDs

As a demonstration of CVI measurements in diseased eyes with choroidal hyper/hypoTDs, patients diagnosed with

2936

Zhou et al. Mitigating hyper/hypoTDs on CVI using OCT
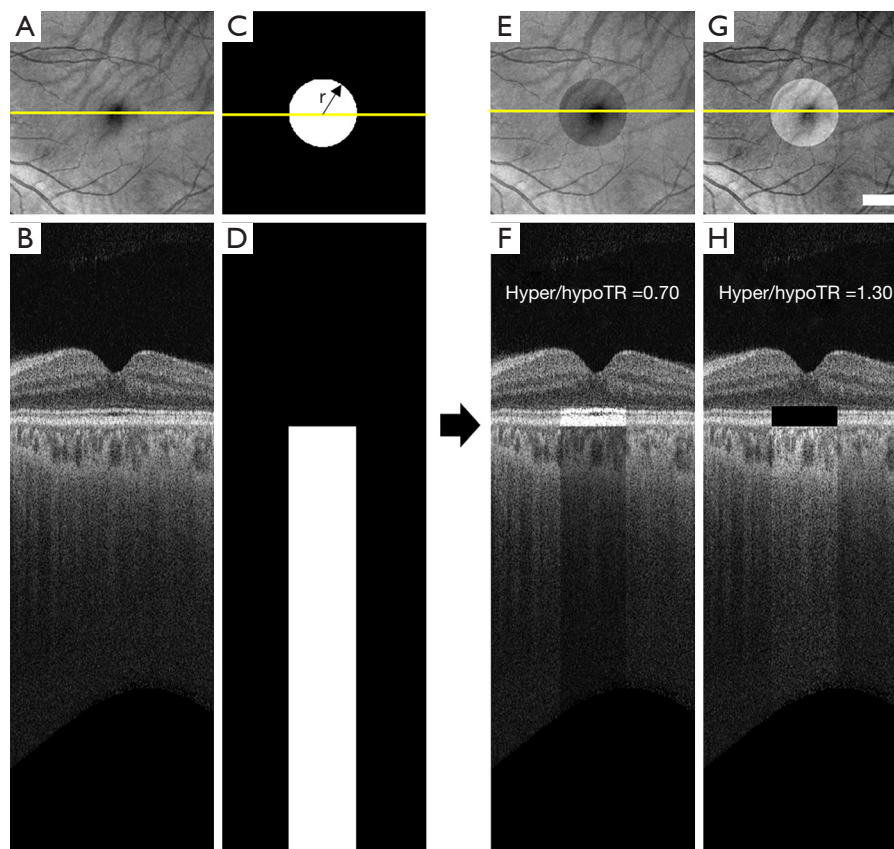
Figure 2 The hyper/hypoTD simulation model. For each SS-OCT scan, a cylindrical region was selected centered at fovea below BM, within which the signal intensities were altered to simulate choroidal hypo-/hyperTDs. Representative enface sub-RPE projection (A,C,E,G), corresponding B-scans (B,D,F,H) were shown for the original scan, the simulation mask, the hypo-transmission simulation and the hyper-transmission simulation, respectively. Scale bar: 1 mm. Hyper/hypoTR, hyper/hypo transmission ratio; hypoTD, hypo-transmission defect; SS-OCT, swept-source optical coherence tomography; BM, Bruch's membrane; hyperTDs, hyper-transmission defects; RPE, retinal pigment epithelium.

GA secondary to non-exudative AMD were enrolled. The atrophic lesion was fully contained within the 6×6 mm scan. *En face* choroidal vasculature maps were generated using a minimum projection as previously reported (28). GA was outlined based on the *en face* sub-RPE images (32). Signal distributions inside and outside the GA lesion, *en face* vasculature maps, and CVI maps were compared with and without attenuation correction.

For CVI measurements in diseased eyes with choroidal hypoTDs, a group of eyes with large drusen (drusen volumes ≥0.03 mm^3) from AMD before and after the drusen spontaneously resolved without evidence of disease progression were enrolled. The same dataset was previously used to validate a compensation method for the CC flow deficit quantification (33). SS-OCT scans from the 2 closest visits before and after drusen resolution were used. CVI was measured on these scans with and without attenuation correction.

Statistical analysis

The data (e.g., age and CVI) were presented as the mean and standard deviation (SD). Nonparametric analysis was utilized to compare the CVI measurements with and without attenuation correction. Statistical analysis was carried out using MATLAB R2018b and IBM SPSS V25 (Armonk, NY, USA), and plots were generated using GraphPad Prism (GraphPad Software, San Diego, CA, USA). Statistical significance is represented at three levels: *, $P \le 0.05$; **, $P \le 0.01$; ***, $P \le 0.001$.

Table 1 Demographics of study groups

Study group	Number of eyes	Number of patients	Age (years) (mean ± SD)
Normal (10)	10	10 (50% were women)	31.1±9.7
Geographic atrophy secondary to nonexudative AMD (34)	38	27 (52% were women)	81.4±7.54
Collapsed drusen (33)	8	8 (62.5% were women)	67.9±2.5

SD, standard deviation; AMD, age-related macular degeneration.
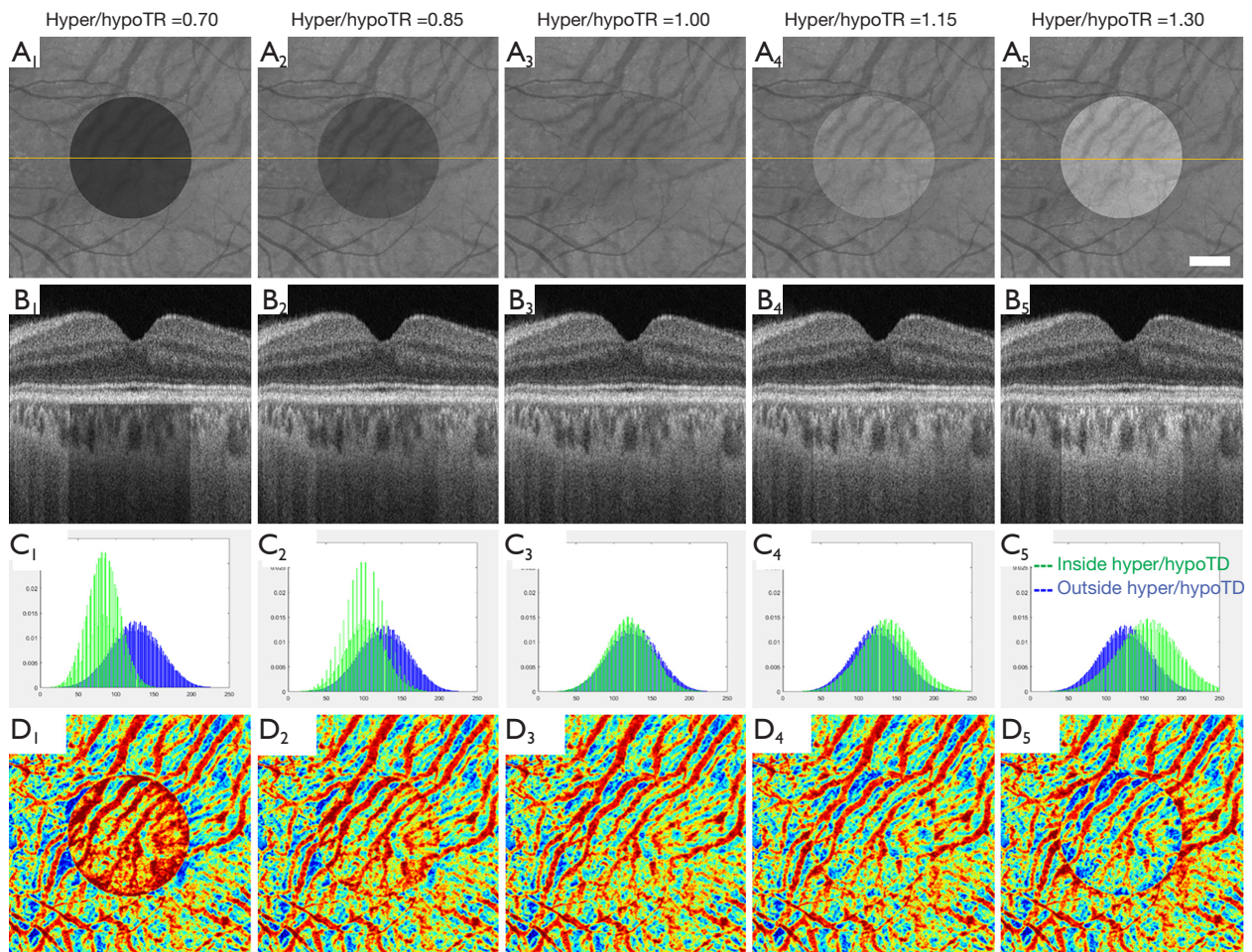
Figure 3 Simulations of hyper/hypo transmission defect model to verify the accuracy of CVI measurements. *En face* images of (A) sub-RPE slab, (B) representative B-scan, (C) histogram of signal intensity and (D) enface CVI map from simulated scans with hyper/hypo transmission ratios (hyper/hypoTRs) equal to 0.70, 0.85, 1.00, 1.15 and 1.30. The third column with a hyper/hypoTR equal to 1 show the results from original scans and is used as the "ground truth". Scale bar: 1 mm. CVI, choroidal vascularity index; RPE, retinal pigment epithelium; hyper/hypoTR, hyper/hypo transmission ratio.

Results

SS-OCT scans of ten normal eyes from ten subjects (age =31.1±9.7 years, AL =24.1±0.91 mm) were collected (*Table 1*). A simulation model was built to alter OCT signals below the RPE in normal eyes to mimic the hyper/hypoTDs in the choroid. As seen in *Figures 3,4*, both the severity (hyper/hypoTR) and the size of hyper/hypoTD region (r)

2938

Zhou et al. Mitigating hyper/hypoTDs on CVI using OCT
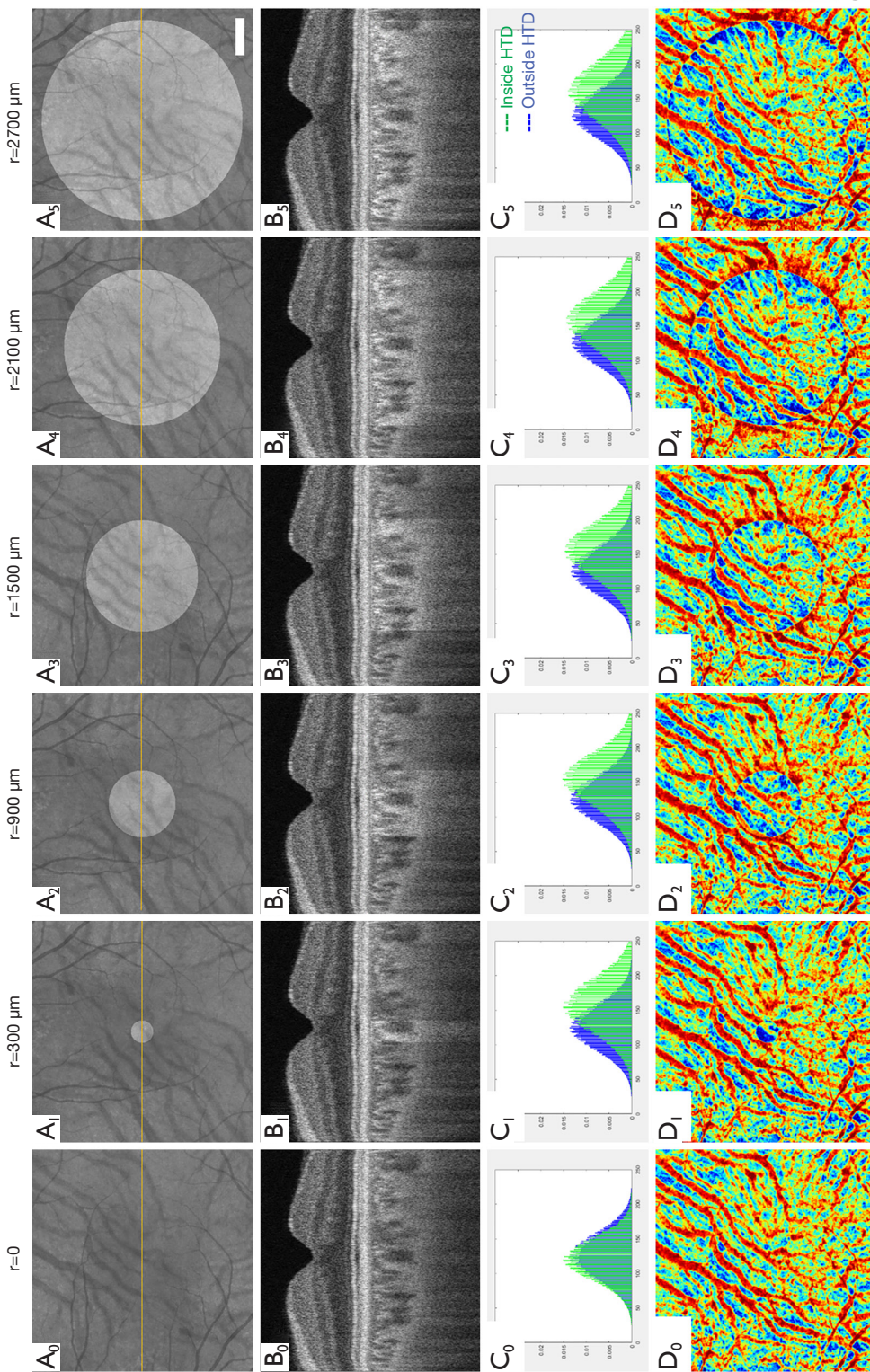
Figure 4 Simulations of choroidal hyperTD model to verify accurate CVI measurements with various sizes of choroidal hyperTDs with a hyper/hypoTR =1.30. *En face* images of (A) a sub-RPE slab, (B) representative B-scan, (C) histogram of signal intensities and (D) *en face* CVI map from simulated scans with r equal to 0, 300, 900, 1,500, 2,100 and 2,700 μm. The left column with r equal to 0 show the results from original scans and is used as "ground truth". Scale bar: 1 mm. HyperTD, hyper-transmission defect; CVI, choroidal vascularity index; hyper/hypoTR, hyper/hypo transmission ratio.
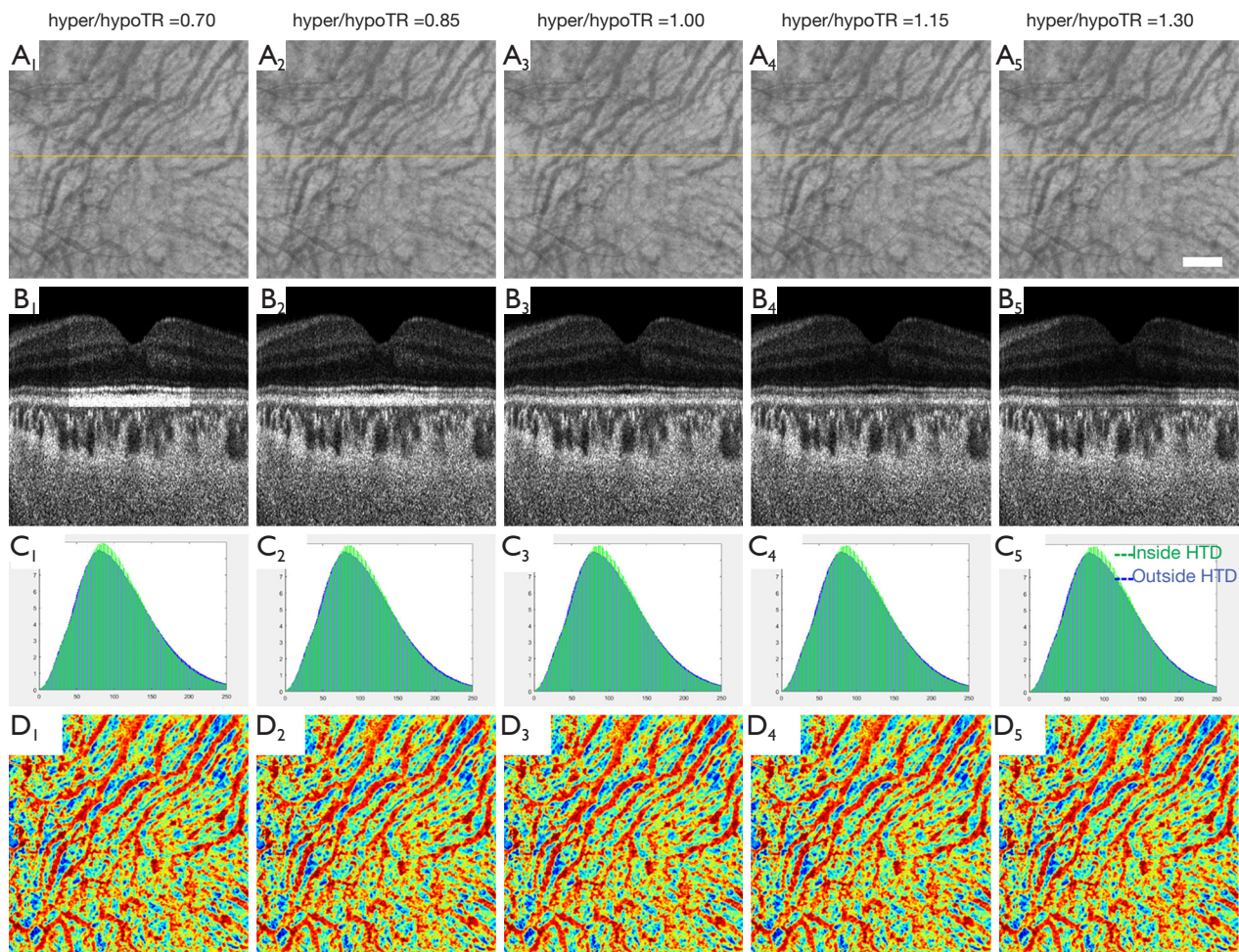
Figure 5 Attenuation correction eliminates the effects of choroidal hyper/hyperTDs. After attenuation correction, the effects of choroidal hyper/hypoTDs were eliminated as seen from *en face* images of (A) the sub-RPE slabs and (B) representative B-scans; (C) resulting in similar histogram signal intensities and (D) *en face* CVI maps with accurate CVI measurements in all simulations with r=1,500 μm and hyper/hypo transmission ratios =0.7, 0.85, 1.15 or 1.3. Scale bar: 1 mm. Hyper/hypoTR, hyper/hypo transmission ratio; hyper/hyperTDs, hyper/hypo transmission defects; RPE, retinal pigment epithelium; CVI, choroidal vascularity index.

affect the CVI quantification. Hyper/hypoTRs equal to 1 correspond to the original scan, which is used to establish the "ground truth". Hyper/hypoTDs in the *en face* images of the sub-RPE slab and in the B-scans were similar to those from diseased eyes, indicating that our model produced realistic simulation of the choroidal hyper/hypoTDs (*Figure 3A,3B*). We observed shifted signal intensity distributions in all hyper/hypoTD regions (*Figure 3C*). CVIs were overestimated in examples with choroidal hypoTDs (*Figure 3D*, D_1,D_2) and underestimated in examples with choroidal hyper-transmission defects (hyperTDs) (*Figure 3D*, D_4,D_5). The influence of hyper/hypoTDs increased as the size

of the region occupied by the lesion increased (*Figure 4*). Interestingly, regions at the edges of the simulated hyper/hypoTDs have an obvious discontinuous CVI, which indicated that the automated binarization would generate incorrect results in these regions at the margins of hyper/hypoTDs (*Figure 4D*, D_1-D_5).

We used attenuation correction to compensate the effects of choroidal hyper/hypoTDs on CVI measurements in the simulated scans and found it to give excellent results (*Figure 5*). Attenuation correction has been used previously to eliminate the shadowing caused by large retinal vessels and to improve the contrast in choroid slabs, and was shown
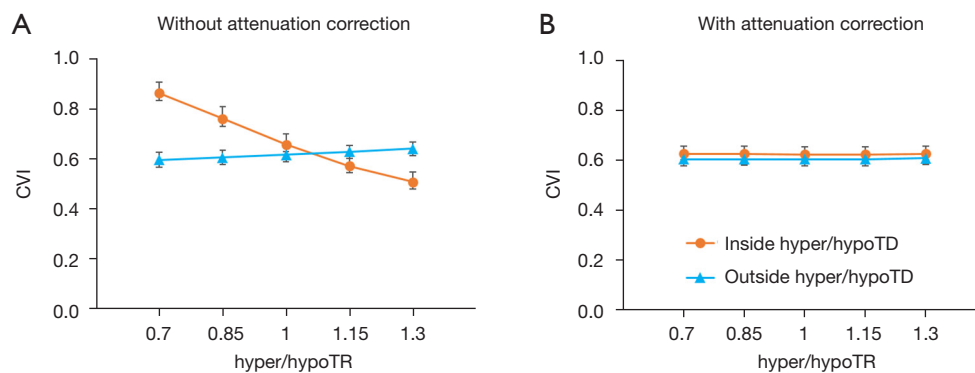
Figure 6 CVI measurements in the presence of hyper/hypoTDs without and with attenuation correction. (A) CVI measurement inside and outside a simulated lesion without attenuation correction; (B) CVI measurements inside and outside simulated lesion with attenuation correction. Hyper/hypoTRs changed from 0.7 to 1.3 to mimic choroidal hyper/hypoTDs. Results of scans with hyper/hypoTR =1, which are the original scans, were used as "ground truth". CVI, choroidal vascularity index; hyper/hypoTDs, hyper/hypo transmission defects; hyper/hypoTRs, hyper/hypo transmission ratios.

to generate more reliable vessel segmentation (28,29). After attenuation correction, differences in signal intensities within the hyper/hypoTD regions were eliminated as shown in the *en face* images of the sub-RPE slabs, B-scans, and signal intensity histograms (*Figure 5A-5C*). CVI maps calculated from simulated scans after attenuation correction were almost identical to those from the original scans with attenuation correction (*Figure 5D*).

We analyzed the effect of hyper/hypoTDs on CVI measurement statistically (*Figure 6*), using the CVI from the original scan as reference. We observed significantly higher CVI measurements in regions with hypoTDs, and the CVI decreased as the hypoTD decreased and significantly lower CVI in regions with hyperTDs and the CVI decreased as the hyperTD increased (all P<0.001). After attenuation correction, CVIs both inside and outside the regions with hyper/hypoTDs were consistent with that of the "ground truth", that is with the measurements from the original scans. With the use of the global thresholding method, hypo/hyperTDs were found to not only affect CVI inside the lesion but also the CVI of normal regions outside the hypo/hyperTDs.

A comparison on the results before and after applying the attenuation correction in GA eyes with hyperTDs (*Table 1*) is shown in *Figure 7*. The histogram of the OCT signals demonstrated that a choroidal hyperTD caused an uneven illumination of choroid structures under and outside atrophy. This resulted in a choroidal shadow within the region of atrophy and discontinuous choroidal vessels seen on the *en face* vasculature map. When extracting dark lumens

that corresponded to choroidal vessels, segmentation resulted in vessels appearing much smaller than they were in the control, resulting in much smaller CVI measurements (*Figure 7A-7E*). With attenuation correction, we observed almost identical pixel intensity distributions under and outside atrophy both in B-scans and in 3D choroid slabs. The *en face* choroidal vasculature showed more continuous vessels across the GA region, meeting the requirement of Otsu's method to segment choroidal vessels successfully (*Figure 7F-7J*).

A quantitative analysis was conducted in eyes with drusen, which cause hypoTDs, and in the same eyes following the spontaneous collapse of drusen (*Figure 8*). The collapse of drusen was identified in 8 eyes from 8 patients (age =67.9±2.5 years, and 62.5% of them were women) (*Table 1*). In these eyes the hypo-transmission associated with drusen at the baseline scans was absent or significantly reduced at the follow up scans, allowing for a natural control. If no compensation was applied, the CVI measured in eyes with drusen was significantly larger than the CVI in eyes after the drusen collapsed (**, P=0.0046). After attenuation correction was applied, there is no significant difference between CVIs before and after the drusen collapsed (n.s., P=0.7527). Attenuation correction not only increased the contrast in the choroidal slab, but also eliminated the choroidal hypoTDs under the drusen in visit 1 (*Figure 8C,8E*). The resulting *en face* CVI maps showed overestimation of CVI due to the shadowing caused by the drusen without attenuation correction when compared with that from the follow-up visit after the drusen
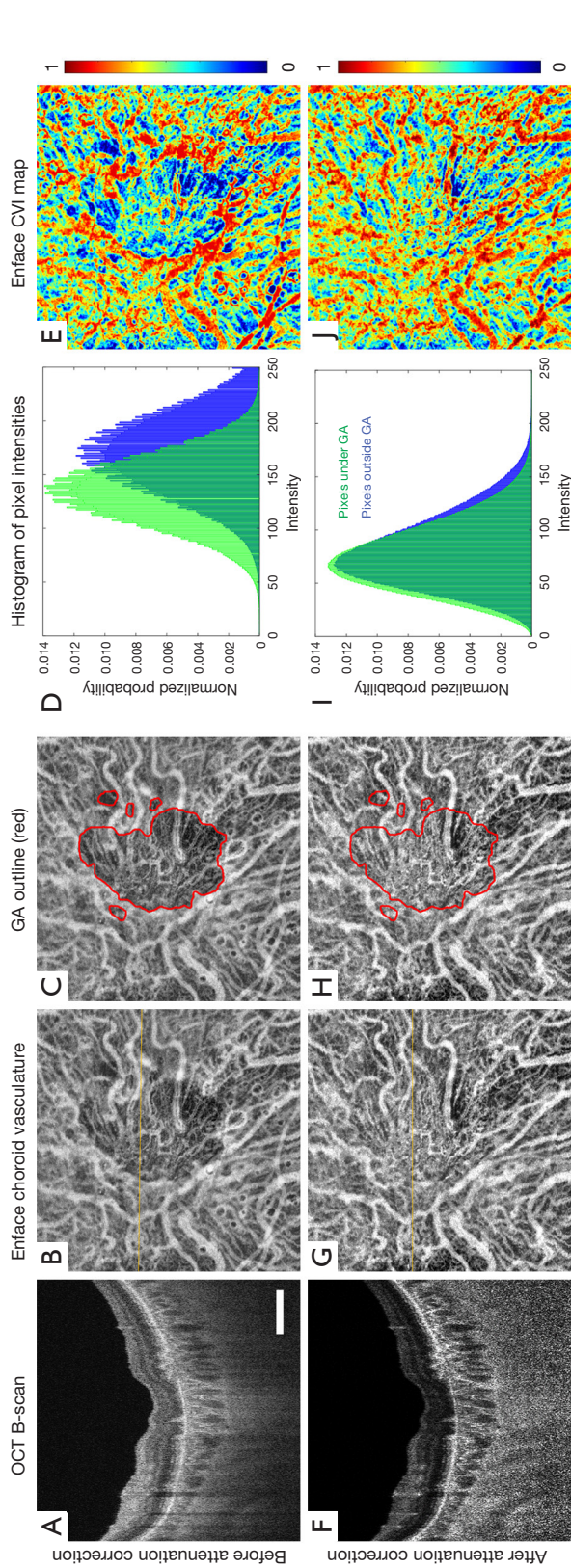
Figure 7 CVI measurements in an eye with GA. (A,F) Representative B-scans (locations indicated by the yellow lines); (B,G) *en face* choroidal vasculature overlaid with manual outline of GA (red line); (D,I) histogram of pixel intensities inside and outside atrophic region and (E,J) *en face* CVI maps with (top row) and without (bottom row) attenuation correction, respectively. Scale bar: 1 mm. OCT, optical coherence tomography; GA, geographic atrophy; CVI, choroidal vascularity index.

2942

Zhou et al. Mitigating hyper/hypoTDs on CVI using OCT
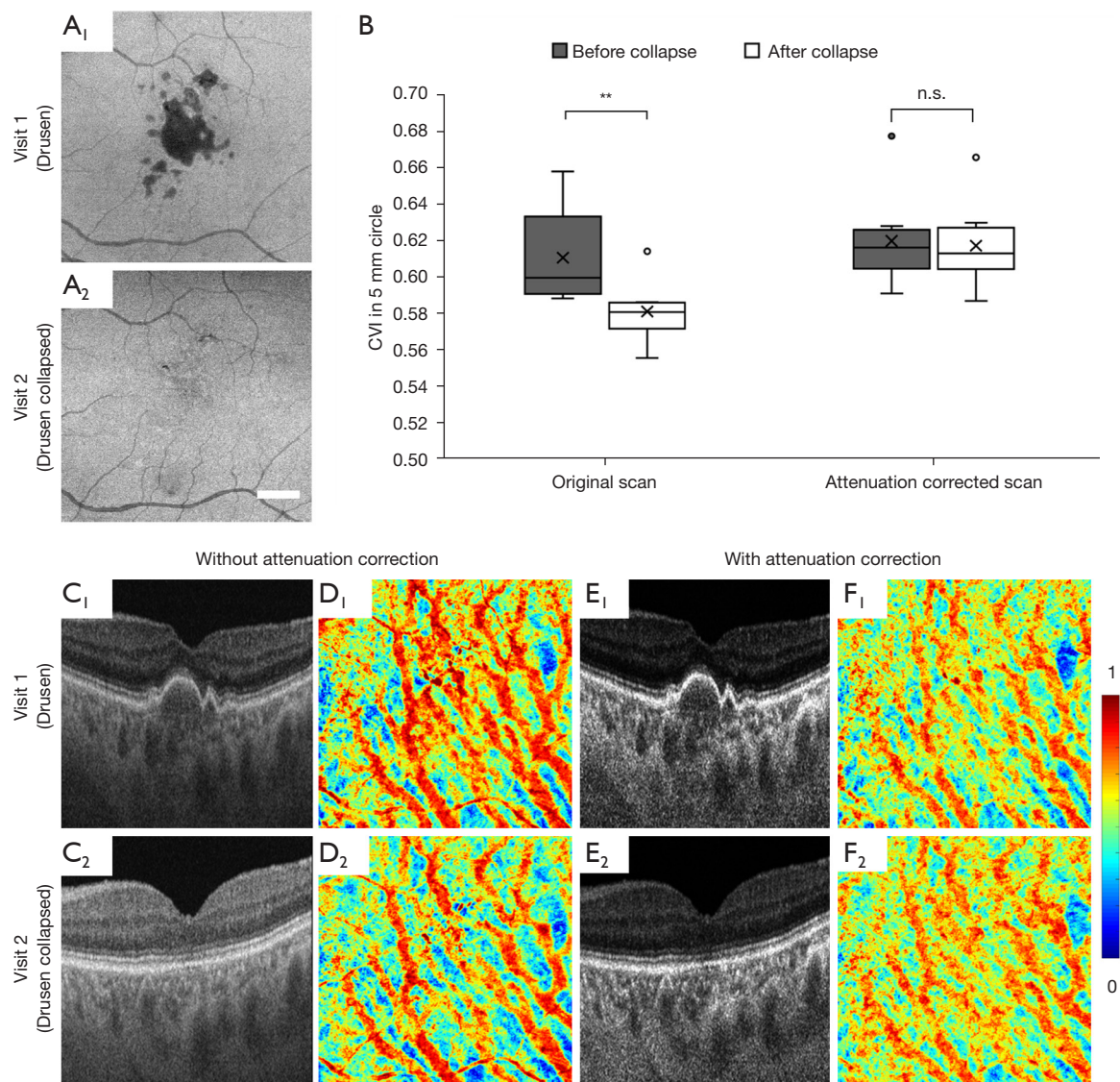
Figure 8 CVI measurements in an eye with drusen before and after the drusen collapsed. (A) *En face* images of RPE slab showed the resolution of drusen; (B) CVI within the 5mm circle region centered at fovea calculated from original SS-OCT scans showed significant difference before and after drusen collapse, while no difference was detected with attenuation correction; (C-F) representative B-scan, CVI maps with and without attenuation correction of scans from two visits respectively. Scale bar: 1 mm. CVI, choroidal vascularity index; RPE, retinal pigment epithelium; SS-OCT, swept-source optical coherence tomography.

collapsed (*Figure 8D*, D_1, D_2). With attenuation correction, CVI maps before and after drusen collapse were consistent.

Discussion

This report provides a strategy for evaluating the ground-truth for choroidal vessel quantification when no objective ground-truth exists. A pseudo-ground-truth was generated by using the CVI measurements from scans of normal eyes and then applying a compensation method when simulating choroidal hyper/hypoTDs. The dataset would be available to standardize CVI measurement methods upon request. A wide range of CVI measurements from around 30% to 60% have been reported with difference scanning systems using various binarization and compensation methods (10,11,21,35). So far, it is not clear whether any

of the methods can provide accurate CVI measurements in eyes with hyper/hypoTDs. For example, one of the most common approaches used ImageJ-based methods to calculate the CVI from a sub-foveal region using a single B-scan acquired using enhanced-depth imaging (EDI) SD-OCT and whose image intensity was normalized using three selected vessel lumens (24). However, it is difficult to decide which three vessel lumens should be selected if there is uneven illumination such as when a hyper/hypoTD is partially included in the region.

Our proposed simulation model could be used to evaluate the behavior of any given approach to CVI measurements in eyes with choroidal hyper/hypoTDs. The simulation model showed that both the severity of the hyper/hypoTD and the size of the lesion affected the CVI measurements. Only after applying appropriate compensation were we able to mitigate the bias caused by hyper/hypoTDs and reproduce the original measurements. We also observed more alterations in CVI measurements at the edges of a lesion (*Figures 3D,4D*). Since the anterior portion of the lesions, such as PED, drusen or GA, is of great interest in disease progression and monitoring, it is worth noting that an appropriate compensation is necessary to measure CVIs in eyes with these lesions that cast a choroidal hyper/hypoTD. While we previously reported the use of attenuation correction as a necessary strategy to segment choroidal vessels by eliminating shadows from retinal vessels and enhancing contrast between choroid vessels and surrounding stroma (28), this current report shows the ability of attenuation correction to compensate for hyper/hypoTDs when measuring the CVI. By applying attenuation correction to normal eyes with simulated hyper/hypoTDs and then applying the attenuation correction to eyes with real diseases that possess these defects such as GA and drusen, we demonstrated that accurate CVI measurements appeared to be achieved in eyes with hyper/hypoTDs after attenuation correction. Based on the histogram of signals inside and outside hyper/hypoTD regions, it can be concluded that the altered signal intensity distribution is the key reason that causes bias in CVI measurements. A shift toward weaker choroidal signal intensities in hypoTDs would result in more or larger dark lumens identified as choroidal vessels, whereas a shift toward stronger choroidal signal intensities in hyperTDs would result in less or smaller dark lumens identified as choroidal vessels. Thus, any compensation method, such as the attenuation correction method studied in this work, that can correct the signal intensity distributions, should be able

to provide more accurate CVI measurements. Recently, the importance of this compensation strategy was shown when we reported that the CVI inside the GA region correlated with the lesion enlargement rate, whereas other choroidal measurements outside the GA region had no significant correlation (34).

On the other hand, this study demonstrated that any cause that alters the light intensity in the choroid, either pathologically or physiologically, could affect the quantification of CVI. This is because that metrics like CVI are dependent on the segmentation of choroidal vessels by the use of dark lumen appearance in OCT scans. Other potential metrics such as fractal dimension and vessel skeleton density which are independent on the width of vessels, may be useful alternates in the future investigations because these metrics are affected less by the alterations in light intensity.

Limitations of this work involve the structure of the simulation model, which assumes an ideal situation where the choroidal hyper/hypoTDs caused by the changes of light penetration into the choroid after passing through the RPE/BM complex and the reflective properties in the choroid beyond remain the same. Signals in the photoreceptor layers are roughly adjusted by assuming the input light is consistent, which may not fully mimic the situation in diseased eyes with pigment aggregation or absence of photoreceptors. In real eye diseases, choroidal tissue may also be altered due to more complicated pathologies such as migrated pigments, accumulated deposits in BM and alterations in choroidal stroma. A more complex hyper/hypo TDs model that better represents disease could be helpful in understanding the optical properties and testing quantification methods in diseased eyes. Secondly, in the simulation model, the hyper/hypoTR is set in a range that reflects the signal intensity change observed in most of the eyes analyzed, in which typically the altered signals neither fall below background noise nor rise above saturation level. In these situations, the attenuation correction algorithm is capable of compensating for the simulated hyper/hypoTDs. In severe cases in which light transmission is significantly attenuated such as in the presence of a large PED or blood anterior to the choroid, current attenuation compensation will not be sufficient. The algorithm will fail if the hypoTD is so severe to reduce the signals in the choroid below the background noise. Another limitation is that we only tested one of the previously reported binarization methods, which is a global thresholding on SS-OCT scans. The hyper/hypoTD simulation model should be able to evaluate other

2944

Zhou et al. Mitigating hyper/hypoTDs on CVI using OCT

local thresholding methods on SD-OCT scans as well.

Conclusions

Overall, the proposed simulation model should be useful in revealing the impact of choroidal hyper/hypoTDs in CVI quantification, and in providing a standard model to validate different CVI quantification methodologies. Qualitative and quantitative analyses on CVIs of eyes with GA or large drusen demonstrated the importance of a compensation strategy such as attenuation correction to ensure accuracy in choroidal vessel segmentation. Only with appropriate compensation should CVI measurements be evaluated in ocular diseases with choroidal hyper/hypoTDs.

Acknowledgments

Footnote

Reporting Checklist: The authors have completed the MDAR checklist. Available at https://qims.amegroups.com/article/view/10.21037/qims-21-1093/rc

Conflicts of Interest: All authors have completed the ICMJE uniform disclosure form (available at https://qims.amegroups.com/article/view/10.21037/qims-21-1093/coif). RKW serves as an unpaid Deputy Editor of *Quantitative Imaging in Medicine and Surgery*. RKW discloses intellectual property owned by the Oregon Health and Science University and the University of Washington, and receives research support from Moptim Inc., Colgate Palmolive Company, and Carl Zeiss Meditec, Inc.; GG receives research support from Carl Zeiss Meditec, Inc. GG and the University of Miami co-own a patent that is licensed to Carl Zeiss Meditec, Inc. PJR receives research support from Carl Zeiss Meditec, Inc. and Stealth BioTherapeutics. He is a consultant for Apellis, Boehringer-Ingelheim, Carl Zeiss Meditec, Chengdu Kanghong Biotech, Ocunexus/

InflammX Therapeutics, Ocudyne, Regeneron, and Unity Biotechnology. And he has equity interest in Apellis, Ocudyne, Ocunexus/InflammX, and Verana Health. He is a consultant to Carl Zeiss Meditec. The other authors have no conflicts of interest to declare.

Ethical Statement: The authors are accountable for all aspects of the work in ensuring that questions related to the accuracy or integrity of any part of the work are appropriately investigated and resolved. The study was conducted in accordance with the Declaration of Helsinki (as revised in 2013). The study was approved by the IRB of Medical Sciences Subcommittee at the University of Miami, Miller School of Medicine and written informed consent was taken from all individual participants.

References

1. Nickla DL, Wallman J. The multifunctional choroid. Prog Retin Eye Res 2010;29:144-68.
2. Yoneya S, Tso MO. Angioarchitecture of the human choroid. Arch Ophthalmol 1987;105:681-7.
3. Linsenmeier RA, Padnick-Silver L. Metabolic dependence of photoreceptors on the choroid in the normal and detached retina. Invest Ophthalmol Vis Sci 2000;41:3117-23.
4. Ring HG, Fujino T. Observations on the anatomy and pathology of the choroidal vasculature. Arch Ophthalmol 1967;78:431-44.
5. Mrejen S, Spaide RF. Optical coherence tomography: imaging of the choroid and beyond. Surv Ophthalmol 2013;58:387-429.
6. Gallego-Pinazo R, Dolz-Marco R, Gómez-Ulla F, Mrejen S, Freund KB. Pachychoroid diseases of the macula. Med Hypothesis Discov Innov Ophthalmol 2014;3:111-5.
7. Cheung CMG, Lee WK, Koizumi H, Dansingani K, Lai TYY, Freund KB. Pachychoroid disease. Eye (Lond) 2019;33:14-33.

8. Singh SR, Vupparaboina KK, Goud A, Dansingani KK, Chhablani J. Choroidal imaging biomarkers. Surv Ophthalmol 2019;64:312-33.

9. Agrawal R, Gupta P, Tan KA, Cheung CM, Wong TY, Cheng CY. Choroidal vascularity index as a measure of vascular status of the choroid: Measurements in healthy eyes from a population-based study. Sci Rep 2016;6:21090.

10. Zhou H, Dai Y, Shi Y, Russell JF, Lyu C, Noorikolouri J, Feuer WJ, Chu Z, Zhang Q, de Sisternes L, Durbin MK, Gregori G, Rosenfeld PJ, Wang RK. Age-related changes in choroidal thickness and the volume of vessels and stroma using swept-source OCT and fully automated algorithms. Ophthalmol Retina 2020;4:204-15.

11. Giannaccare G, Pellegrini M, Sebastiani S, Bernabei F, Moscardelli F, Iovino C, Napoli PE, Campos E. Choroidal vascularity index quantification in geographic atrophy using binarization of enhanced-depth imaging optical coherence tomographic scans. Retina 2020;40:960-5.

12. Kim M, Ha MJ, Choi SY, Park YH. Choroidal vascularity index in type-2 diabetes analyzed by swept-source optical coherence tomography. Sci Rep 2018;8:70.

13. Tan R, Agrawal R, Taduru S, Gupta A, Vupparaboina K, Chhablani J. Choroidal vascularity index in retinitis pigmentosa: an OCT study. Ophthalmic Surg Lasers Imaging Retina 2018;49:191-7.

14. Ratra D, Tan R, Jaishankar D, Khandelwal N, Gupta A, Chhablani J, Agrawal R. Choroidal structural changes and vascularity index in stargardt disease on swept source optical coherence tomography. Retina 2018;38:2395-400.

15. Tan KA, Laude A, Yip V, Loo E, Wong EP, Agrawal R. Choroidal vascularity index—a novel optical coherence tomography parameter for disease monitoring in diabetes mellitus? Acta Ophthalmol 2016;94:e612-6.

16. Agrawal R, Chhablani J, Tan KA, Shah S, Sarvaiya C, Banker A. Choroidal vascularity index in central serous chorioretinopathy. Retina 2016;36:1646-51.

17. Agrawal R, Li LK, Nakhate V, Khandelwal N, Mahendradas P. Choroidal vascularity index in vogt-koyanagi-harada disease: an EDI-OCT derived tool for monitoring disease progression. Transl Vis Sci Technol 2016;5:7.

18. Ting DSW, Yanagi Y, Agrawal R, Teo HY, Seen S, Yeo IYS, Mathur R, Chan CM, Lee SY, Wong EYM, Wong D, Wong TY, Cheung GCM. Choroidal remodeling in age-related macular degeneration and polypoidal choroidal vasculopathy: a 12-month prospective study. Sci Rep 2017;7:7868.

19. Kirby MA, Li C, Choi WJ, Gregori G, Rosenfeld P, Wang R. Why choroid vessels appear dark in clinical OCT images. Proc SPIE Ophthalmic Technologies XXVIII 2018;10474:1047428.

20. Liu X, Bi L, Xu Y, Feng D, Kim J, Xu X. Robust deep learning method for choroidal vessel segmentation on swept source optical coherence tomography images. Biomed Opt Express 2019;10:1601-12.

21. Vupparaboina KK, Dansingani KK, Goud A, Rasheed MA, Jawed F, Jana S, Richhariya A, Freund KB, Chhablani J. Quantitative shadow compensated optical coherence tomography of choroidal vasculature. Sci Rep 2018;8:6461.

22. Sonoda S, Sakamoto T, Kakiuchi N, Shiihara H, Sakoguchi T, Tomita M, Yamashita T, Uchino E. Semi-automated software to measure luminal and stromal areas of choroid in optical coherence tomographic images. Jpn J Ophthalmol 2018;62:179-85.

23. Wei X, Sonoda S, Mishra C, Khandelwal N, Kim R, Sakamoto T, Agrawal R. Comparison of choroidal vascularity markers on optical coherence tomography using two-image binarization techniques. Invest Ophthalmol Vis Sci 2018;59:1206-11.

24. Sonoda S, Sakamoto T, Yamashita T, Uchino E, Kawano H, Yoshihara N, Terasaki H, Shirasawa M, Tomita M, Ishibashi T. Luminal and stromal areas of choroid determined by binarization method of optical coherence tomographic images. Am J Ophthalmol 2015;159:1123-1131.e1.

25. Ferrara D, Silver RE, Louzada RN, Novais EA, Collins GK, Seddon JM. Optical coherence tomography features preceding the onset of advanced age-related macular degeneration. Invest Ophthalmol Vis Sci 2017;58:3519-29.

26. Zhang Q, Zheng F, Motulsky EH, Gregori G, Chu Z, Chen CL, Li C, de Sisternes L, Durbin M, Rosenfeld PJ, Wang RK. A novel strategy for quantifying choriocapillaris flow voids using swept-source oct angiography. Invest Ophthalmol Vis Sci 2018;59:203-11.

27. Rinella NT, Zhou H, Zhang Q, Keiner C, Oldenburg CE, Duncan JL, Wang RK, Schwartz DM. Quantifying choriocapillaris flow voids in patients with geographic atrophy using swept-source oct angiography. Ophthalmic Surg Lasers Imaging Retina 2019;50:e229-35.

28. Zhou H, Chu Z, Zhang Q, Dai Y, Gregori G, Rosenfeld PJ, Wang RK. Attenuation correction assisted automatic segmentation for assessing choroidal thickness and vasculature with swept-source OCT. Biomed Opt Express 2018;9:6067-80.

29. Girard MJ, Strouthidis NG, Ethier CR, Mari JM. Shadow removal and contrast enhancement in optical coherence

tomography images of the human optic nerve head. Invest Ophthalmol Vis Sci 2011;52:7738-48.

30. Yin X, Chao JR, Wang RK. User-guided segmentation for volumetric retinal optical coherence tomography images. J Biomed Opt 2014;19:086020.

31. Otsu N. A threshold selection method from gray-level histograms. IEEE Transactions on Systems, Man, and Cybernetics 1979;9:62-6.

32. Thulliez M, Zhang Q, Shi Y, Zhou H, Chu Z, de Sisternes L, Durbin MK, Feuer W, Gregori G, Wang RK, Rosenfeld PJ. Correlations between choriocapillaris flow deficits around geographic atrophy and enlargement rates based on swept-source OCT imaging. Ophthalmol Retina 2019;3:478-88.

33. Shi Y, Chu Z, Wang L, Zhang Q, Feuer W, de Sisternes L, Durbin MK, Gregori G, Wang RK, Rosenfeld PJ. Validation of a compensation strategy used to detect choriocapillaris flow deficits under drusen with swept source OCT angiography. Am J Ophthalmol 2020;220:115-27.

34. Shi Y, Zhang Q, Zhou H, Wang L, Chu Z, Jiang X, Shen M, Thulliez M, Lyu C, Feuer W, de Sisternes L, Durbin MK, Gregori G, Wang RK, Rosenfeld PJ. Correlations between choriocapillaris and choroidal measurements and the growth of geographic atrophy using swept source OCT imaging. Am J Ophthalmol 2021;224:321-31.

35. Agrawal R, Wei X, Goud A, Vupparaboina KK, Jana S, Chhablani J. Influence of scanning area on choroidal vascularity index measurement using optical coherence tomography. Acta Ophthalmol 2017;95:e770-5.